Title	Hybrid density functional theory description of N- and C-doping of NiO
Author(s)	Nolan, Michael; Long, R.; English, N. J.; Mooney, D. A.
Publication date	2011-06-10
Original citation	Nolan, M., Long, R., English, N. J., Mooney, D. A. (2011) 'Hybrid density functional theory description of N- and C-doping of NiO', Journal of Chemical Physics, 134, 224703. http://dx.doi.org/10.1063/1.3596949
Type of publication	Article (peer-reviewed)
Link to publisher's version	http://dx.doi.org/10.1063/1.3596949 Access to the full text of the published version may require a subscription.
Rights	© 2011, AIP Publishing. This article may be downloaded for personal use only. Any other use requires prior permission of the author and AIP Publishing. The following article appeared in M. Nolan et al. J. Chem. Phys. 134, 224703 (2011) and may be found at http://dx.doi.org/10.1063/1.3596949
Item downloaded from	http://hdl.handle.net/10468/2919

Hybrid Density Functional Theory Description of N- and C-Doping of NiO

Michael Nolan[*]

Tyndall National Institute, University College Cork, Lee Maltings, Prospect Row,

Cork, Ireland

michael.nolan@tyndall.ie

Run Long, Niall J. English[*] and Damian A. Mooney

The SEC Strategic Research Cluster and the Centre for Synthesis and Chemical

Biology, Conway Institute of Biomolecular and Biomedical Research, School of

Chemical and Bioprocess Engineering, University College Dublin, Belfield, Dublin 4,

Ireland

niall.english@ucd.ie

Abstract: The large intrinsic band gap of NiO hinders its potential application as a photo-catalyst under visible-light irradiation. In this study, we have performed first-principles screened exchange hybrid density functional theory with the HSE06 functional calculations of N- and C-doped NiO to investigate the effect of doping on the electronic structure of NiO. C-doping at an oxygen site induces gap states due to the dopant, the positions of which suggest that the top of the valence band is made up primarily of C 2p-derived states with some Ni 3d contributions, and the lowest-energy empty state is in the middle of the gap. This leads to an effective band gap of 1.7 eV, which is of potential interest for photocatalytic applications. N-doping induces comparatively little dopant-Ni 3d interactions, but results in similar positions of dopant-induced states, *i.e.*, the top of the valence band is made up of dopant 2p states and the lowest unoccupied state is the empty gap state derived from the dopant, leading to band gap narrowing. With the hybrid DFT results available, we discuss issues with the DFT+U description of these systems.

Introduction

Metal oxides are widely used in key technologies, such as catalysis, gas sensors, dielectrics, photochemistry, and electrochemistry [1, 2]. In the growing area of renewable energy, including the hydrogen economy, photocatalytically active metal oxides are of great interest for hydrogen production via water splitting. TiO_2 is considered the paradigm photocatalytically active metal oxide, but has a wide band gap (~3.2 eV for anatase [3] and 3.05 eV for rutile [4]) that favours absorption of ultra violet light, thus makeing undoped TiO_2 unsuitable for photocatalysis. Substitutional cation and anion doping of TiO_2 have been pursued as approaches to extend light absorption into the visible-light region.

A widely studied example is N-doped TiO_2, for which experimental and theoretical methods have been used [5, 6] and this is a good photocatalytic material. C-doped TiO_2 also shows good photocatalytic efficiency under visible-light [7] and has also been theoretically studied. Theoretical studies allow one to investigate the atomic level details of the impact of doping on the structure and electronic structure of a metal oxide. Besides being potentially useful for band gap modulation of metal oxides, substitutional doping can also be used to enhance reactivity in chemical reactions [8, 9]. A further motivation to study doping in metal oxides more closely is to address fundamental aspects, including the choice of modelling approach, dopant incorporation, dopant and host oxidation states and charge compensation, which require closer scrutiny and have been lacking in many previous studies.

Besides TiO_2, there are other metal oxides that could be used in photocatalytic applications [10]. NiO has generated interest as a catalyst for electrochemical applications such as electrolysers, fuel cells, and batteries [11, 12]. NiO-loaded semiconductors have been used

extensively as photocatalysts for water splitting due to the NiO-support interface being an important factor in determining the photoefficiency. The pioneering work of Zou et al. [13] introduced water splitting for stoichiometric H_2 and O_2 evolution over $NiO_x/In_{0.9}Ni_{0.1}TaO_4$ photocatalysts under visible light irradiation. Following this work, Hu et al. [14] reported that $NiO/SrBi_2O_4$ could effectively decompose pathogenic bacteria under visible light irradiation. Zou et al. [15] controlled the NiO-support interface of NiO-loaded photocatalysts such as NiO/Ta_2O_5 and NiO/ZrO_2 that were prepared with plasma treatment, and found that high photocatalytic activity. On the other hand, investigations of $NiO/NiAl_2O_4$ as oxygen carriers for chemical-looping combustion to fabricate high effective gaseous fuels have been performed in several papers [16, 17].

The experimental band gap of undoped NiO is *ca.* 3.8 eV, which leads to absorption of ultra violet radiation [18]. In analogy to TiO_2 [19], it is possible that substitutional anion-doping with elements such as N or C may narrow the band gap of NiO, but as far as we are aware, such studies have not been performed. In addition, the description of NiO with the commonly used approximate exchange-correlation potentials in density functional theory (DFT) is a challenge, so much so, that the standard approximate DFT exchange correlation functionals cannot even describe qualitatively the electronic structure of NiO [20, 21], describing incorrectly the nature of the valence band of NiO.

DFT corrected for on-site Coulomb interactions (DFT+U), applied to the Ni 3d states [22, 23] is one approach to go beyond DFT in describing oxide metal and has been used to provide a reasonable description of the band gap, magnetic moments and lattice parameters of NiO [–24 - 27].However, due to the persistent band gap underestimation for reasonable values of U,

DFT+U can have issues in the prediction of defect-induced levels in the oxide band gap. This can arise, since the +U correction is usually applied to the host cation states incorrectly described with DFT, under an assumption that such a correction is not necessary for the dopant electronic states. This assumption may lead to an incorrect interpretation of where the dopant-induced electronic states are found .

Recently, screened exchange hybrid DFT [28] in a plane-wave basis set has become an alternative approach to describe consistently metal oxide systems where DFT fails [29 - 31], and has been applied successfully to the study of NiO [32]. While plane-wave hybrid DFT is burdened with a significant increase in computational expense compared to DFT or DFT+U, studies with this approach are generally more accurate and can be used to check on the predictions of doped materials from other levels of theory.

In this paper, we present a study of pure bulk NiO, and C- and N-doped NiO using screened exchange hybrid DFT, comparing with a previous DFT+U study [27]. Bulk NiO is studied since previous work has considered bulk NiO [27,32] and understanding doping of the bulk oxide is necessary before proceeding to study doping of models of the films and surfaces that are generally present in an experimental sample. Using both hybrid and DFT+U, an insulating description of NiO is obtained and doping with C and N introduces new dopant-derived states into the band gap of the oxide, which may be beneficial for narrowing the band gap of NiO. However, our results show that a DFT+U description of doped NiO is still problematic and more generally, the presence of localised defect states may lead to reduced photo-efficiencies. In this respect, parallel experimental research to assess the viability of using doped NiO for photocatalytic applications would be worthwhile.

Methodology

The hybrid DFT calculations were performed using a plane-wave basis set as implemented in the VASP code [33,34]. The plane wave cut-off energy was set at 400 eV. The projector augmented wave (PAW) [35] approach is used to describe the core-valence interaction, with an [Ar] core on Ni and a [He] core and C, N and O. The hybrid screened exchange HSE06 [28] functional was used for all systems in this paper, i.e. undoped NiO, C and N doped NiO and the species used in the calculation of formation energies. With the hybrid DFT methodology used here, exact exchange is included with a contribution of 25 %. The choice of an appropriate value for this contribution is important, and 20 % exact exchange was originally derived by Becke [36] by fitting to atomization energy data of a large number of molecular species. Later work by Perdew et al. [37] derived an exact exchange contribution of 25 %, and subsequent work is summarized in [38]. While material properties such as band gap can be most accurately described with values different to 25% exchange, deviations from this value tend to be quite small and it is taken as a universally applicable parameter. In the screened exchange formulation of hybrid DFT, the full Hartree-Fock exchange interaction is screened, with a universal screening parameter of 0.11 Bohr^{-1} [28]. Thus, in principle, hybrid DFT contains adjustable parameters, similar to DFT+U, although the exact exchange contribution and the screening length are generally taken to be universal. It is possible that the remaining deficiencies in the screened exchange hybrid DFT approach as used in this paper arise from using the universal exact exchange contribution and screening length. However there are two primary differences that make hybrid DFT a superior approach: (i) the inclusion of exact

exchange is for all species and all angular momentum, so that all species are treated on an equal footing, whereas the +U term is added for a particular angular momentum term for a given species, e.g. Ni 3d (ii) the values of the exchange contribution and screening length are universal, whereas in DFT+U, a different U value should be used depending on the material under investigation and even the property of interest in the calculation.

In previous DFT+U calculations [27], the Perdew-Wang 1991 approximate generalized gradient approximation to the exact exchange-correlation functional (PW91) was used, and we used values of U – J = 5.3 eV, with U = 6.3 eV and J = 1 eV; U is the effective on-site Coulomb repulsion parameter and J is the exchange parameter. This was applied to Ni 3d electrons, having been used in earlier studies [32, 39].

A Monkhorst–Pack k-point sampling mesh [40] of $4 \times 4 \times 4$ was used for all calculations. The atomic positions were optimized until the residual forces were below 0.02 eV/Å, while the NiO bulk lattice constants were determined from a Murnaghan equation-of-state fit to a set of constant volume simulations.

We performed substitutional doping of one lattice oxygen atom by a carbon or nitrogen atom, giving the possibility of singlet or triplet spin configurations for C-doping and doublet or quartet spin configurations for N-doping, as controlled by the VASP keyword, NUPDOWN. These spin configurations are relative to the initial AFM spin ordering of the NiO host. During relaxation, we do not constrain the Ni spins to retain their AFM configuration. For C-doping, the triplet configuration is the most stable and for N-doping the doublet configuration is the most stable; in a later section we discuss the change in the spins of the Ni atoms upon doping. The structures considered are constructed from a $(2 \times 2 \times 2)$ 64-atom NiO

supercell and relaxed until the forces were less than 0.02 eV/Å. Replacing a single O atom by a single dopant corresponds to 1.56 atom % doping concentration.

3. Results and discussion

3.1 Undoped Bulk NiO

Firstly we compare the computed lattice constants of pure NiO. With HSE06, the lattice constant is computed to be 4.195 Å, compared to 4.16 Å with DFT+U [27] and 4.17 Å from experiment [41]. Both DFT+U and HSE06 provide good lattice constants for bulk NiO.

The band gap calculated from HSE06 is 4.2 eV, comparing reasonably with the experimental band gap in the range 3.8 - 4 eV [42, 43], showing a small overestimation with HSE06, and comparing more favourably than the strongly underestimated DFT+U band gap, which is 2.6 eV [27]. HSE06 can overestimate band gaps of metal oxides, e.g. for TiO_2 [44] or d^6 spinels [45], so this finding is not so unusual.. This finding is consistent with the now comprehensive literature in which comparisons of the band gaps of solids from DFT, DFT+U and hybrid DFT are available. Since it rectifies some of the issues present with standard DFT, hybrid DFT generally produces band gaps that are in better agreement with experiment compared with DFT. While a small overestimation of the band gap is found using the standard HSE06 parameters for some systems, the hybrid DFT band gaps are more consistent with experiment and the positions and nature of defect states can be determined with confidence.

With DFT+U, a large enough value of U can be computed in order to reproduce the experimental band gap, but this generally requires such a large U that it leads to a severe

deterioration of other material properties. The effect of U is limited to the particular species and angular momentum selected, while the hybrid DFT correction is applied to all species and all electronic states.

The ground state of NiO is antiferromagnetic (AFM) and the AFM type-II ordering is shown schematically in Figure 1(a), with successive (111) planes showing an alternating spin. This AFM ordering for NiO is well known [43].The HSE06 local magnetic moment on the Ni ion is 1.65 μ_B which is consistent with the experimental value of 1.64 μ_B [41] and the previous DFT+U result of 1.68 μ_B [27].

The total electronic density of states (EDOS) for pure NiO is shown in Figure 1 (b), comparing HSE06 and DFT+U. The most obvious difference between the two approaches is the energy gap between the valence band and the conduction band. In addition, there are some qualitative differences between the EDOS for the two approaches. In particular there are extra peaks at the top of the VB and the bottom of the CB from the DFT+U description. The origin of this comes from the use of DFT+U, where U is applied only to the Ni 3d states and is not large enough to give the same band gap as experiment. A larger U on Ni or a U applied to O 2p could of course achieve this, but at a cost of degrading other properties, such as lattice constant and Ni magnetic moment. With the value of U used, the Ni 3d states in the valence band still lie too high in energy, being found at the top of the VB and the charge-transfer character of NiO is not fully described. In contrast, with HSE06, the Ni 3d states lie lower in energy and are more consistent with experiment.
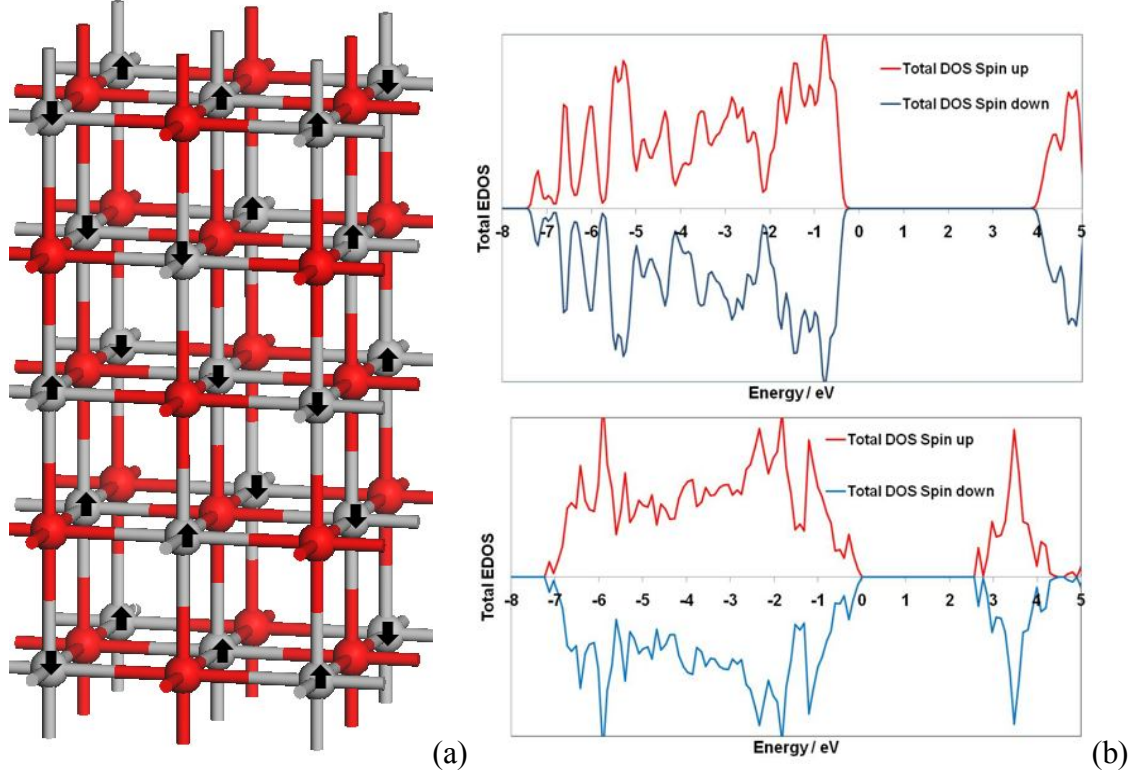
Figure 1. (a) Rock salt structure of undoped NiO showing a schematic of the AFM ordering found in undoped NiO. The black arrows show the spin directions, Ni is grey and oxygen is red (b) Total electronic density of states (EDOS) for undoped NiO. The top panel of part (b) shows the HSE06 total EDOS and the bottom panel shows the DFT+U total EDOS.

3.2 Doping of Bulk NiO

For doping, we firstly investigate the energy cost to incorporate the dopants onto an O site in the NiO lattice; due to the symmetry of the cubic structure, all O sites are equivalent. The formation energies for doping are calculated according to formula (1):

$$E_{form} = E(X@O) - E(NiO) - \mu_X + \mu_O \tag{1}$$

This ap proach was also used in our earlier DFT+U study [27]. In this calculation,

$E(X@O)$ is the total energy of NiO containing the dopant X (C or N) and $E(NiO)$ is the total energy of the pure 64-atom NiO supercell. μ_O is the chemical potential for the substituted O and μ_X is the chemical potential of the incorporated species, X. The formation energy depends on the growth conditions, which can be varied from O- to Ni-rich, and the chemical potentials of O and Ni must satisfy the relationship $\mu_{Ni} + \mu_O = \mu_{NiO}$. Under O-rich conditions, the chemical potential μ_O is determined by half the total energy of an isolated O_2 molecule. Under Ni-rich conditions, where metallic Ni would be precipitated, μ_{Ni} is the energy of one Ni atom in bulk Ni ($\mu_{Ni} = \mu_{Ni}^{metal}$) and μ_O in this case is computed from the formation energy of bulk NiO and μ_{Ni}. For C and N dopants, the chemical potentials μ_C and μ_N were computed from $\mu_C = \mu(CO_2) - 2\mu_O$ and $\mu_N = \mu(NO_2) - 2\mu_O$, respectively. If we use NO instead of NO_2 to determine μ_N, then we find a small increase of 0.2 eV in the formation energy of N-doped NiO, which is negligible compared to the magnitude of the formation energy in table 1.

E_{form}	O-rich	Ni-rich
N@O	8.30 (6.5)	5.97 (3.0)
C@O	8.64 (12.5)	6.31 (9.0)

Table 1. Formation energies (eV) of N- and C-doped NiO. Previous DFT+U results [27] are given in parentheses.

The calculated formation energies under Ni- and O-rich growth conditions are given in Table 1, with the DFT+U results given in parenthesis. While both methods show quite high

formation energies for each dopant, these are for bulk NiO and one would expect that in NiO films, in which surfaces are present, doping would be easier, so these results should be considered an upper limit to the formation energies. While there are differences in the absolute energies between DFT+U and hybrid DFT, the energies from both approaches show that: 1) substitution of O by N is thermodynamically favoured over substitution of O by C under both Ni- and O-rich growth conditions; 2) substitution of either dopant on the oxygen site is more favourable under reducing conditions and 3) the difference between the formation energies for C and N doping is rather small.

Some reasons behind the relative formation energies are as follows. The differences in the ionic radii of C, N and O, which decrease in the order: C^{4-} (2.60 Å) > N^{3-} (1.71 Å) > O^{2-} (1.40 Å). This suggests that incorporating the larger dopant on the oxygen site will have an energy cost associated with it and that substituting N on an O site will be more favourable than incorporation of C on an O site. One could also consider the corresponding bulk system of NiC and NiN, which are Ni_3C and Ni_3N. While we have not found bond strengths for Ni-C/Ni-N in the literature, the bulk systems of Ni_3N and Ni_3C have formation enthalpies that are very similar, being 0.3 eV [46, 47], compared to 3 eV for NiO [48]. Therefore Ni-O bonding is stronger than Ni-C and Ni-N bonding, which is reflected in the formation energies for substitutional doping. The magnitude of the formation energies between C and N doping are also rather small, consistent with the similar bulk Ni_3N and Ni_3C formation energies. The bond distances are for Ni-C and Ni-N in Ni_3C [49] and Ni_3N [50] are 1.90 Å and 1.89 Å, respectively; but this does not give any further insights to the stabilities of the doped structures.

The computed Bader charges [51] are -1.10 |e| on C and -1.37 |e| on N, indicating the formation of C^{2-} and N^{2-} anions upon doping. With the different oxidation states of C and N compared to O in NiO, we have to consider the formation of compensating defects as follows. For C-doping, the dopant has two fewer electrons than the oxygen it replaces, so that a single neutral oxygen vacancy will compensate the dopant by donating two electrons to allow C to obtain a closed shell C^{4-} oxidation state. For N-doping, the dopant has one less electron than the oxygen it replaces, so that two dopants accompanied by a neutral oxygen vacancy are required for charge compensation.

For C-doping, the most stable compensating oxygen vacancy structure has a formation energy of +3.71 eV (compared to +4.77 eV that we compute for bulk NiO). This means that an oxygen vacancy will not readily form to compensate the dopant. In the case of N-doping, we found that positioning the dopants in neighbouring anion sites is the most stable distribution. The most stable compensating oxygen vacancy site then has a formation energy of +2.39 eV. Thus, N-doping will also not necessarily be compensated by the formation of an oxygen vacancy. Subsequent results are therefore presented for substitutionally-doped NiO.

Ni Atom	C-Ni	μ_{Ni}/ Bohr	N-Ni	μ_{Ni}/ Bohr
1	2.21 (2.08)	+1.65	2.26 (2.06)	+1.65
2	2.16 (2.07)	+1.65	2.26 (2.05)	+1.65
3	2.06 (2.05)	-1.42	2.26 (2.05)	+1.65
4	2.01 (2.04)	-1.28	2.11 (2.05)	-1.52

| 5 | 1.99 (1.98) | +1.57 | 2.11 (2.04) | -1.52 |
| 6 | 1.99 (1.97) | -1.25 | 2.11 (2.03) | -1.52 |

Table 2: Dopant-Ni distances (Å) and Ni magnetic moments for Ni atoms neighbouring the dopant site. Previous DFT+U geometries [27] are given in parentheses. The Ni-O distance in undoped NiO is 2.10 Å.

The local structure around the N and C dopants in the NiO lattice is shown in Figure 2. In this and subsequent figures, Ni ions are blue spheres, oxygen ions are red spheres, and the dopant is a black sphere. Upon examination of the local structure around the dopants, for which Ni-dopant distances are shown in Figure 2 (for reference, the Ni-O distance in undoped bulk NiO is 2.10 Å), we see that while both dopants perturb the local atomic structure around their lattice site, there are some differences between the effect of C- and N-doping on the local atomic structure. For both dopants, the hybrid DFT dopant-Ni distances are longer than the DFT+U distances, the latter show more uniform dopant-Ni distances. In the hybrid DFT solution, both dopants show at least two strongly elongated dopant-Ni distances, which are 2.23 and 2.16 Å for C-Ni and three N-Ni distances of 2.26 Å, which shows that a distortion around the dopant site occurs to accommodate the dopant and its aliovalent oxidation state. For N as dopant, other dopant-Ni distances are a little longer than the Ni-O distance, at 2.11 Å, while for C as dopant, the remaining dopant-Ni distances are shorter than the Ni-O distance.
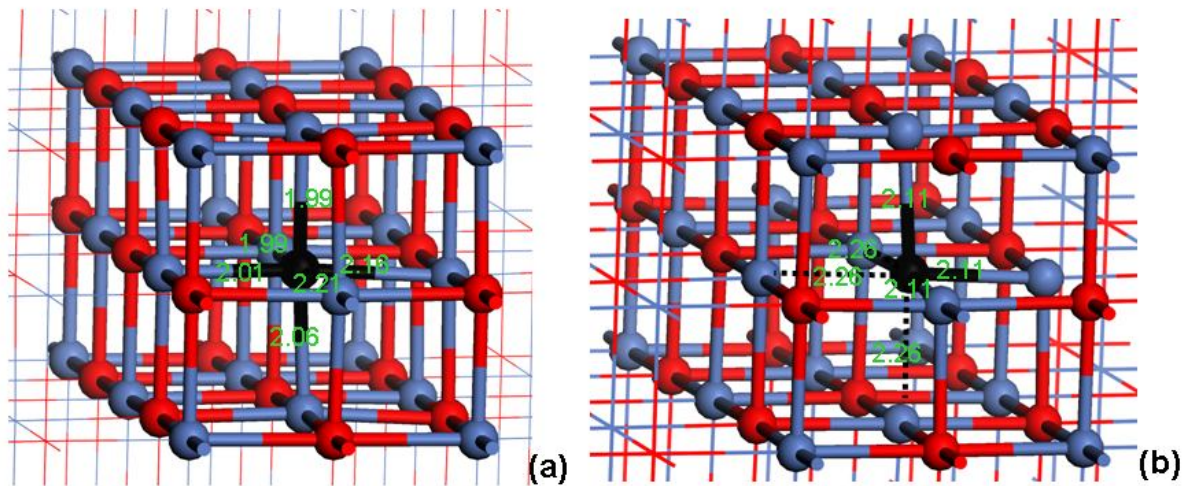
Figure 2. Local geometry of dopant for (a) C- and (b) N-doping of NiO. The pertinent geometry data are given in Table 2. Ni is shown as blue spheres, O as red spheres and the dopant as black spheres. In (b), the dashed black lines indicate the long N-Ni bonds.

To examine the effect of doping on the electronic structure of NiO, we firstly note that upon relaxation, the Ni atoms retain their AFM ordering from the undoped structure. Figures 3 and 4 show the electronic density of states (EDOS) for NiO doped with C and N, respectively. These figures show the total EDOS and the EDOS projected onto the Ni 3d and dopant 2p states (PEDOS). The EDOS is shown over a narrow energy range around the valence and conduction bands to highlight the contributions to the EDOS in these regions. The zero of energy is the Fermi level. Table 2 presents the Ni magnetic moments after doping for the Ni atoms neighbouring the dopant – Ni atoms away from the dopant are unaffected.
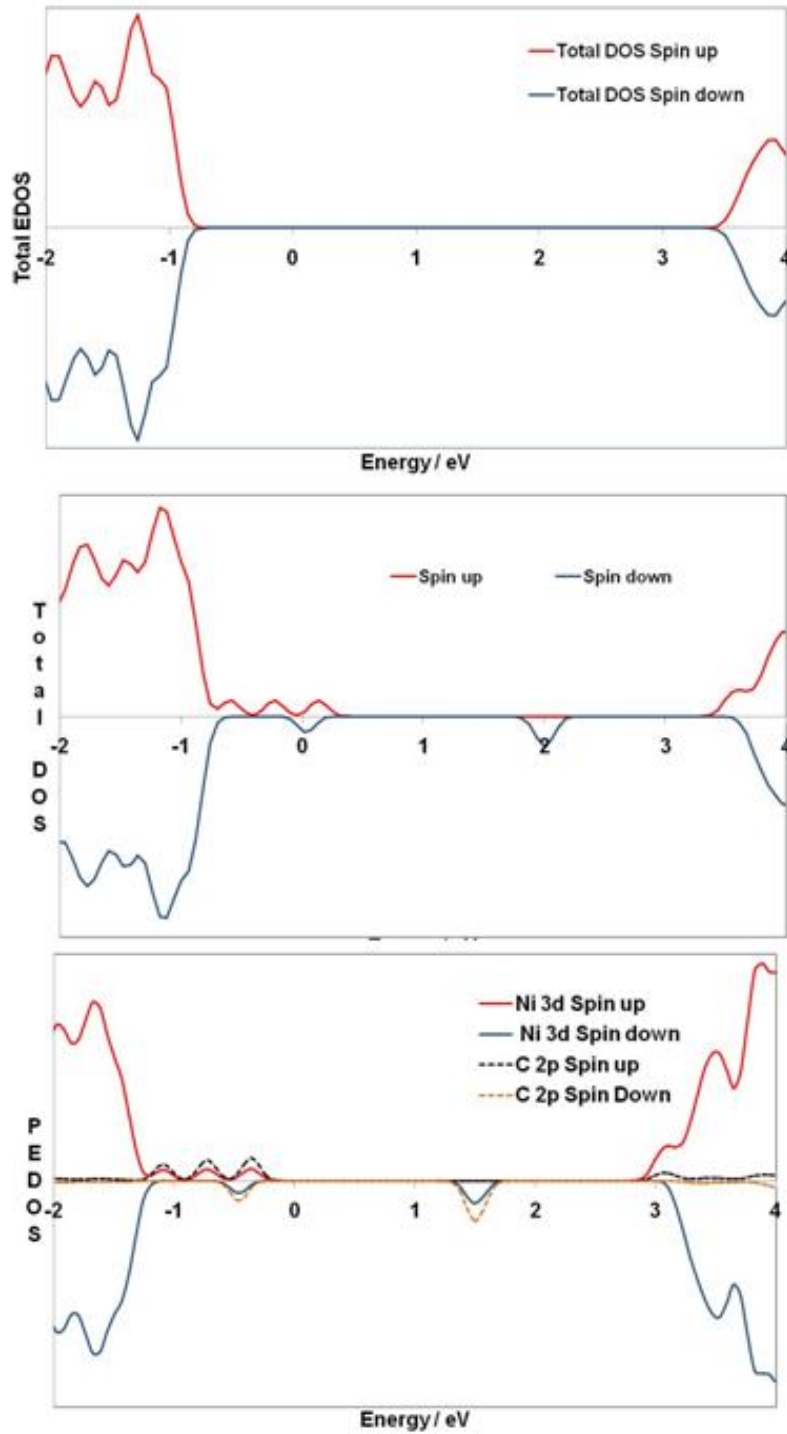
Figure 3. Electronic density of states (EDOS) for C-doped NiO. Top panel: total EDOS of undoped NiO; Middle panel: total EDOS of C-doped NiO (PEDOS); Bottom panel: EDOS projected onto Ni 3d and C 2p states; the latter are multiplied by a factor of 5 to make them more visible relative to Ni

Turning first to the magnetic moments, as outlined in the methods section, although we began from the AFM ground states of undoped NiO and then incorporated the dopant, we did not constrain the Ni spins to keep the AFM ordering. On examining the Ni magnetic moments after doping, the oxide maintains the AFM ordering. Some Ni atoms neighbouring the dopant show a change in magnetic moment upon doping, as shown in table 2, indicating a different interaction between Ni and C/N compared with the interaction between Ni and O. However, the AFM ordering of the Ni magnetic moments does not change and the change in the magnitude of the magnetic moments is relatively small. The dopants both show a small magnetic moment, 0.5 μ_B, when incorporated into the NiO host. However, a discussion of any magnetic interactions in these systems is outside the scope of the present paper.

When carbon is doped into the oxide, the total EDOS shows new states appearing in two different regions of the original band gap. The relative positions of the oxide valence band (VB) and conduction band (CB) edges remain unchanged by doping. The first states of interest lie between the top of the valence band (VB), and the Fermi level (set to 0 eV), so that they are occupied. This now positions the highest occupied states of the doped oxide above the VB of the host oxide. These states arise primarily from occupied C 2p states, with an Ni 3d contribution, as evidenced in the EDOS in and are spin polarised on both C and Ni, giving an excess of occupied spin up states reflected in the magnetic moment on C (see above). The essentially symmetric Ni EDOS around the valence and conduction band edges indicates that the AFM ordering is unchanged and changes in the magnitude of the Ni magnetic moments are small. In analogy to work on other oxides, these dopant derived states could result in narrowing of the effective band gap as they are electronic states from which an electron can

be excited upon illumination.

The second state of interest is a spin-down unoccupied state in the middle of the band gap, which originates from the remaining unoccupied C 2p states, with an Ni 3d contribution. An electron may be excited into this empty state. Thus the effective band gap of NiO could be reduced to *ca.* 1.8 eV for excitation from occupied defect to unoccupied defect states upon C-doping.

In Figure 4, we show the PEDOS for N-doped NiO. The introduction of the dopant leads to the formation of a number of states in the band gap, The first state is a predominantly dopant-derived state which forms at the top of the valence band; upon closer examination, this state shows a small excess of spin up over spin down and gives a magnetic moment on N. Similar to C doping, the Ni EDOS is symmetric and for the same reason. There is also another state, occupied with one electron, marginally above this state. These states are occupied, lying below the Fermi level and form the highest occupied states of the doped oxide.

There is an unoccupied, dopant-induced state *ca.* 1.7 eV above the top of the highest occupied state, which forms the lowest unoccupied states of the doped oxide. Thus, the effective band gap of the oxide could be narrowed towards the visible light region by the presence of N as a dopant There is also another unoccupied Ni 3d state at the bottom of the CB. Similar to C doping, there are small Ni contribution to the gap states.
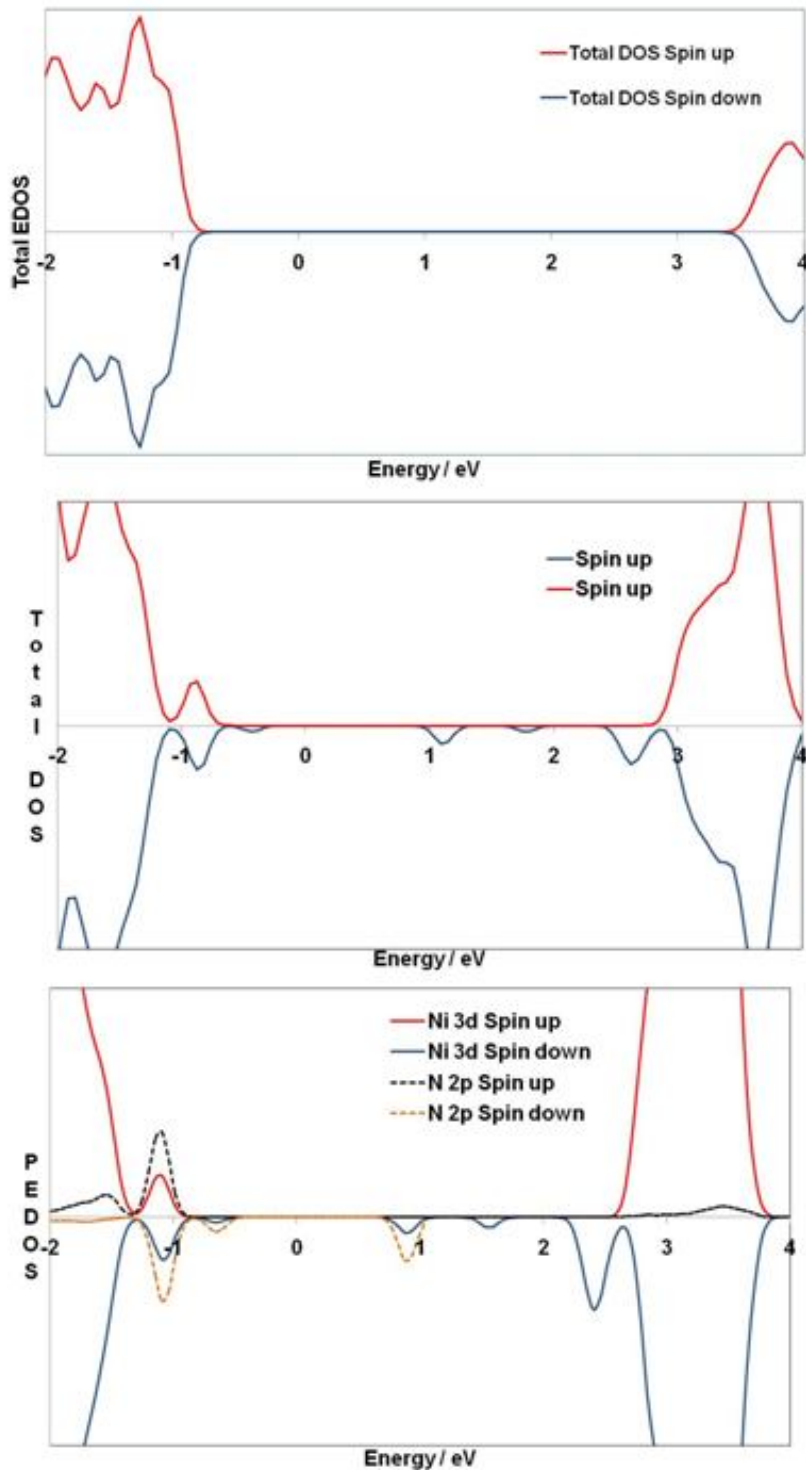
Figure 4. Electronic density of states (EDOS) for N-doped NiO. Top panel: total EDOS of undoped NiO; Middle panel: Total EDOS of N-doped NiO Bottom panel: EDOS projected onto Ni 3d and N 2p states; the latter are multiplied by a factor of 5 to make them more visible relative to Ni.
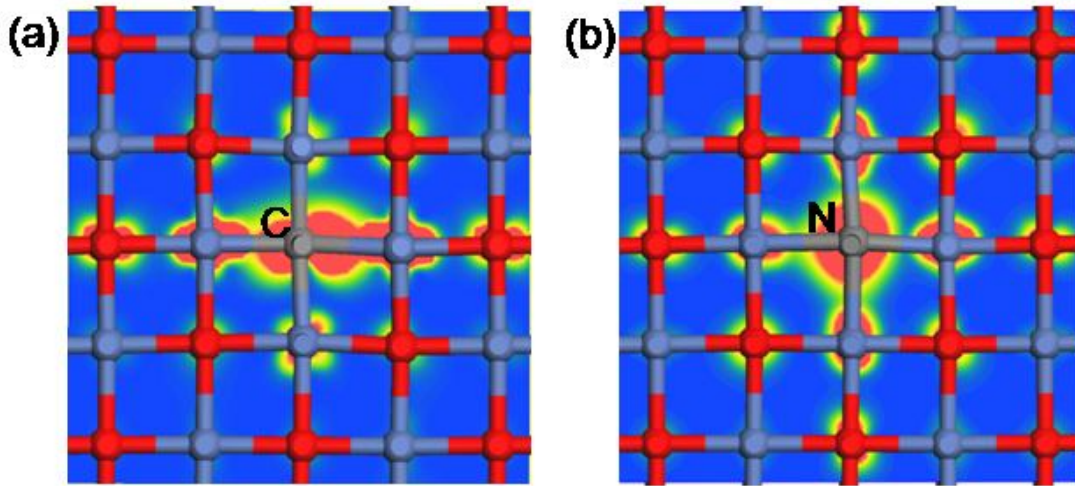
Figure 5: Partial charge density plots taken in a (100) plane including the dopant (which is indicated) and neighbouring Ni atoms for the dopant induced electronic states above the valence band for C and N doped NiO. (a): C doped NiO (b): N doped NiO. In both structures, the dopant is the grey sphere. The magnitude of the charge density goes from a minimum in blue to a maximum in red.

To analyse the contributions to the defect states at the valence band in doped NiO, Figure 5 shows a partial charge density in the energy range of the occupied gap states at the valence band, with a slice taken through a (100) plane containing the dopant and the neighbouring Ni ions in the same plane (although not shown, there are contributions from the remaining two Ni atoms that lie perpendicular to this plane). For both dopants the charge density plots show a predominant contribution from the dopant 2p states. There are also contributions from two Ni atoms directly neighbouring C, with little contribution from the remaining Ni atoms, in particular those with the elongated C-Ni distances. The Ni atoms directly neighbouring N, also contribute to the charge density in this region, with the charge density around the Ni

polarised towards the Ni atoms with the longest N-Ni distances. These charge density plots indicate an interaction between the dopant and the host cations in the local region around the dopant site, which suggests that the new electronic states are quite localised.

3.3 Comparison with DFT+U

To compare with our previous DFT+U results, we show in Figure 6 the Ni 3d and dopant 2p PEDOS for C- -doped NiO computed from DFT+U [27]. The DFT+U description shows that doping introduces new states at the valence band maximum (VBM) with an unoccupied state at the bottom of the CB. The effective band gap is estimated to be *ca.* 1.3 eV. However, there are some notable differences between the DFT+U and hybrid DFT descriptions of C-doping of NiO. With hybrid DFT, the C 2p states at the top of the VB are well separated from the oxide-derived VB, which has been pushed lower in energy, as a consequence of the wider band gap found with hybrid DFT. However, with DFT+U the C 2p states mix strongly with the upper valence band states of the oxide. This arises from the unsatisfactory treatment by standard DFT and DFT+U of the description of the separation between the occupied and unoccupied states in NiO and in the dopant. Introducing the Hubbard U parameter opens up the band gap in NiO, but unless a very large, unphysical U is used, the band gap will generally still be underestimated. At the same time, the positions of the dopant energy states are also suspect and in fact determining the correct relative position of the dopant and host states within a DFT+U approach is problematic. On the other hand, hybrid DFT gives essentially the correct energy gap for the oxide and the correct positions of the dopant electronic statesand

the consequence of this is clear in the position of the occupied C 2p states at the VB, where they are separated from the oxide valence band.

In relation to the empty electronic states, their position relative to the bottom of the CB is rather different when comparing DFT+U and hybrid DFT – in the former these states are at the bottom of the CB, but with HSE, they are positioned well inside the band gap, offset by 1.5 eV from the bottom of the CB.
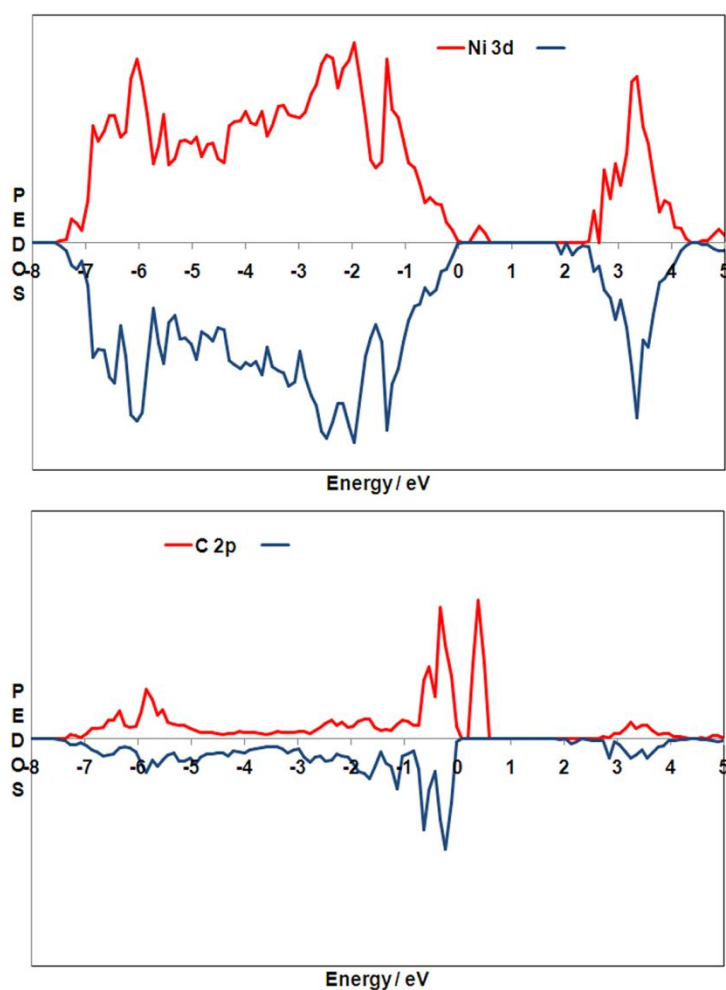

Figure 6: DFT+U EDOS projected onto Ni 3d and C 2p states for C doped NiO.

For N-doped NiO, the EDOS of which is shown in Figure 7, there are similar differences between the two DFT methods. The problems with the NiO band gap discussed above for

DFT+U will also be present in this case. Although both methods place occupied N 2p states at the top of the VB, with DFT+U these interact strongly with the oxide VB states, giving quite different electronic states when compared with hybrid DFT. The unoccupied N 2p states are also positioned differently in the band gap, similar to C-doped NiO. With DFT+U, the unoccupied dopant states are at the bottom of the CB, but are offset from the CB by 1.2 eV with HSE06.
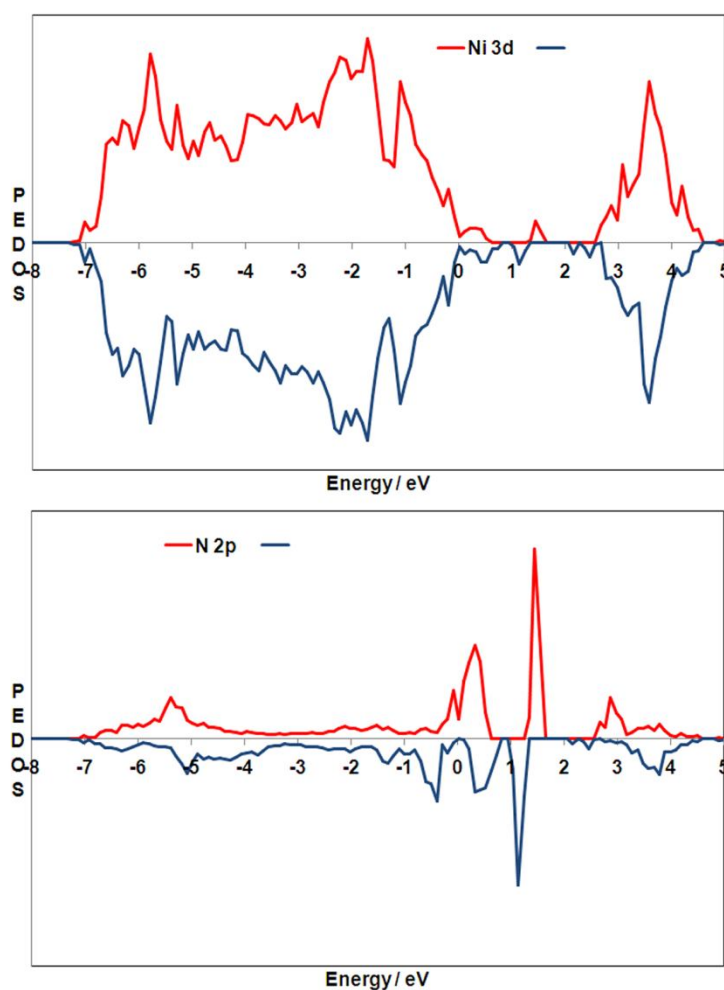

Figure 7: DFT+U EDOS projected onto Ni 3d and N 2p states for N doped NiO.

Although hybrid DFT shows that C- and N-doping in NiO both result in new electronic states at the top of the NiO VB, and lead to effective band gaps that may be useful for

improved visible light absorption compared to undoped NiO, both dopants also result in the formation of quite localised states in the band gap, as in Figure 5. This is of importance, since the presence of localised recombination centres, which can trap charges, will reduce the efficiency of any photocatalytic system, even if photon absorption can be optimised. In contrast to DFT+U, which shows dopant states mixed with the valence and conduction bands, the hybrid DFT solution shows a well-defined localised 2p state for both dopants in the band gap that would serve as a recombination centre. Although our previous DFT+U study and the current work shows that band gap narrowing leads to qualitatively similar effective band gaps (1.3 and 1.7 eV for N-doped NiO with DFT+U and HSE06, respectively), both of which are significantly smaller than the band gap of pure NiO (4.2 eV for hybrid DFT and 2.6 eV from our previous DFT+U results), the poorer description of the unoccupied electronic states with DFT+U could lead to erroneous interpretations of the utility of NiO in photocatalysis.

4. Conclusions

HSE06 calculations of undoped NiO show a band gap of 4.2 eV, in excellent agreement with experiment and superior to standard DFT and our previous DFT+U study [27]. When doping with C on an oxygen site, we find dopant-derived gap states, and their positions suggest that the top of the VB is now made up of C 2p-derived states, with some Ni 3d contributions, and the lowest-energy empty state is in the middle of the gap. This results in an effective band gap of 1.7 eV, which should be suitable for photocatalytic applications. With N-doping, there is less dopant-Ni 3d interaction but a similar set of dopant-induced states result, namely that the top of the VB is now made up of dopant 2p states and the lowest

unoccupied state is the empty gap state induced by the dopant.

In conclusion, based on first-principles calculations and analysis of the electronic structures of N- and C-doped NiO, it was found that both N and C induce 2p impurity states into the band gap, which can narrow the band gap significantly; experimental confirmation of these results would be useful. It would be expected that N-doped NiO would exhibit a higher degree of photocatalytic efficiency than that of C-doped NiO under visible-light irradiation because of the greater presence of isolated, unoccupied states for carriers in C-doped NiO, although N-doped titania also has such states present. Although hybrid DFT does offer an improved description of NiO vis-à-vis DFT+U, ground-state DFT is limited in its treatment of charge dynamics upon visible light excitation.

5. References

[1] V. E. Henrich, P. A. Cox, *The Surface Science of Metal Oxides*; Cambridge University Press: Cambridge, England, 1994.

[2] A. L. Linsebigler, G. Lu, J. T. Yates, Chem. Rev. **95**, 735 (1995)

[3] H. Tang, F. Levy, H. Berger and P. E. Schmid, Phys. Rev. B **52,** 7771 (1995)

[4] J. Pascual, J. Camassel and H. Mathieu, Phys. Rev. B **18,** 5606 (1978)

[5] R. Asahi, T. morikawa, T. Ohawaki, K. Aoki, Y. Taga, Science **293**, 269 (2001).

[6] H. Irie, Y. Watanabe, K. Hashimoto, J. Phys. Chem. B **107**, 5483 (2003).

[7] X. B. Chen, C. Burda, J. Am. Chem. Soc. **130**, 5018 (2008).

[8] M. Nolan, J. Phys. Chem. C, **113,** 2425 (2009)

[9] A. Roldan, M. Boronat, A. Corma and F. Illas, J. Phys. Chem. C, **114,** 6511 (2010)

[10] F. E. Osterloh, Chem Mat., **20,** 35 (2008)

[11] C. N. R. Rao and B. Raveau, *Transition Metal Oxides,* VCH, New York, 1995

[12] A. L. Linsebigler, G. Lu and J. T. Yates, Chem. Rev. **95**, 735 (1995)

[13] Z. G. Zou, J. H. Ye, K. Sayama and H. Arakawa, Nature **414,** 625 (2001)

[14] C. Hu, X. X. Hu. J. Guo, and J. H. Qu, Environ. Sci. Technol, **40,** 5508 (2006).

[15] J. J. Zou, C. J. Liu, and Y. P. Zhang, Langmuir **22**, 2334 (2006).

[16] E. Jerndal, T. Mattisson, and A. Lyngfelt, Energy & Fuels **23**, 665 (2009).

[17] H. Bo Zhao, L. M. Liu, B. W. Wang, D. Xu, L. L. Jiang, and C. G. Zheng, Energy & Fuels **22**, 898 (2008).

[18] P. A. Cox, *Transition Metal Oxides: An Introduction to their Electronic Structure and Propertie*s; The International Series of Monographs on Chemistry Vol. 27; Claredon

Press: Oxford, U.K., 1995.

[19] C. Di Valentin, E. Finazzi, G. Pacchioni, A. Selloni, S. Livraghi, M. C. Paganini, E.

Giamello, Chem Phys., **44,** 339 **(**2007)

[20] V. I. Anisimov, M. A. Korotin and E. Z. Kurmaev, J. Phys.: Condens. Matt. **2,** 3973

(1990)

[21] V. I. Anisimov, I. V. Solovyev, M. A. Korotin, M. T. Czyzyk and G. A. Sawatzky, Phys.

Rev. B, **48,** 16929 (1993)

[22] S. L. Dudarev, G. A. Botton, S. Y. Savarsov, C. J. Humphreys and A. P. Sutton, Phys.

Rev. B, **57,** 1505 (1998)

[23] V. I. Anisimov, J. Zaanen and O. K. Andersen, Phys Rev B, **44,** 943 (1991)

[24] S. L. Dudarev, L-M. Peng, S. Y. Savrasov and J-M. Zuo, Phys. Rev. B **61,** 2506 (2000)

[25] O. Bengone, M. Alouani, P.Blöchl and J. Hugel, Phys. Rev. B **62**, 16392 (2000)

[26] A. Rohrbach, J.Hafner and G. Kresse, Phys. Rev. B **69** 075413 (2004)

[27] R. Long, N. J. English and D. A. Mooney, Physics Letters A **374**, 1184 (2010)

[28] B. J. Janesko, T. M. Henderson and G. E. Scuseria, Phys. Chem. Chem. Phys., **11,** 443,

(2009**)**

[29] P. Agoston, K. Albe, R. Nieminen, and M. J. Puska, Phys. Rev. Lett., **103,** 145501 (2009)

[30] D. O. Scanlon, B. J. Morgan, G. W. Watson and A. Walsh, Phys. Rev. Lett., **103,** 096405

(2009)

[31] M. V. Ganduglia-Pirovano, J. L. F. da Silva and J. Sauer, Phys. Rev. Lett., **102,** 026101

(2009)

[32] P. R. de Moreira, F.Illas and R. L. Martin Phys. Rev. B **65** 155102 (2002).

[33] G. Kresse and J. Hafner, Phys. Rev. B **47**, 558 (1994)

[34] G. Kresse and J. Furtherműller, Phys. Rev. B **54**, 11169 (1996)

[35] P. E. Blöchl, Phys Rev B, **50,** 17953 (1994)

[36] A. D. Becke, J. Chem. Phys. **98,** 1372 (1993).

[37] J. P. Perdew, M. Ernzerhof and K. Burke, J. Chem. Phys **105**, 9982 (1996).

[38] F. Cora, M. Alfredsson, G. Mallia, D. Middlemiss, W.C. Mackrodt, R. Dovesi, R, Orlando, Struct Bond **113,** 171 (2004)

[39] N. Yu, W. B. Zhang, N. Wang, Y. F. Wang, and B. Y. Tang, J. Phys. Chem. C **112,** 452 (2008).

[40] H. J. Monkhorst and J. D. Pack, Phys. Rev. B **13**, 5188 (1976)

[41] G. A. Sawatzky and J. W. Allen, Phys. Rev. Lett. **53**, 2339 (1984)

[42] A. K. Cheetham and D. A. O. Hope, Phys. Rev. B **27**, 6964 (1983)

[43] N. Mironova-Ulmane, A. Kuzmin, M. Cestelli Guidi, M. Piccinini and A. Marcelli, phys. Stat. Sol. (c) **2,** 704 (2005)

[44] P. Deak, B. Aradi and Th. Frauenheim, Phys. Rev. B, **83,** 155207 (2011)

[45] D. O. Scanlon and G. W. Watson, Phys. Chem. Chem. Phys., 2011, doi:10.1039/c0cp02562c

[46] B. A. Kermark, H. Johanson, B. Roos and U. Wahlgren, J. Am. Chem. Soc. **101,** 5876 (1979)

[47] J. S Gibson, J. Uddin, T. R Cundari, N. K Bodiford and A. K Wilson, J. Phys.: Condensed Matter, **22,** 445503 (2010)

[48] R. D. Holmes, H. St. C. O'Neill and R. A. Arculus, Geochim. et Cosmochim. Acta, **11,**

2439 (1986)

[49] I.R. Shein, N.I. Medvedeva and A.L. Ivanovskii, Physica B, **371,** 126 (2006)

[50] A. Leinweber, H. Jacobs, S. Hull, Inorg. Chem., **40,** 5818 (2001)

[51] G. Henkelman, A. Arnaldsson, and H. Jónsson, Comput. Mater. Sci. **36**, 254 (2006)